FINITE ELEMENT MODELING OF PLASTIC DEFORMATION DURING SPIN FORMING OF ALUMINUM 6061-O

Elizabeth Urig, *PhD Candidate*, University of Virginia

Leonid Zhigilei, *Advisor*, University of Virginia

Abstract

Spin and flow forming are metal deformation techniques in which a disk or tube of material is radially thinned and axially lengthened over a rotating mandrel. A finite-element continuum model (FEM) based on commercial software (DEFORM®) was developed to determine the stress/strain distribution and damage accumulation in a flow-formed, near-net-shape part. Computational validation and experimental verification of the model was leveraged to assess the effectiveness of computer simulations. Quantitative comparisons between experimental and computational results show promise for applying a FEM to the flow forming process. Experimental failure locations correlated well with computed damage gradients, and there was good agreement between the measured and predicted roller forces during forming.

1. Introduction

The Advanced Air Transport Technology (AATT) project at NASA Langley Research Center is pursuing the implementation of single-piece, integrally-stiffened cylinders (ISCs) for commercial aircraft fuselages. The ISCs can be fabricated by flow-forming, a process that spins a metallic preform at high speeds and uses rollers to shape the preform around a rotating mandrel. Successful ISC manufacture using Al 6061 and Al 2219 has produced prototypes at both the small (43 cm) and large (3 m) diameter scale[1–3]. The schematic in Figure 1 illustrates the structural features of two full-scale ISCs joined together[4].

Currently, there are no computational models capable of simulating the complex plastic deformation and variable strain fields created in flow-formed cylinders with integral stiffeners[5, 6]. The ability to predict the resultant stress or strain distribution, and identify key points in the process that control material evolution, would ultimately benefit both processing and service properties of ISCs.

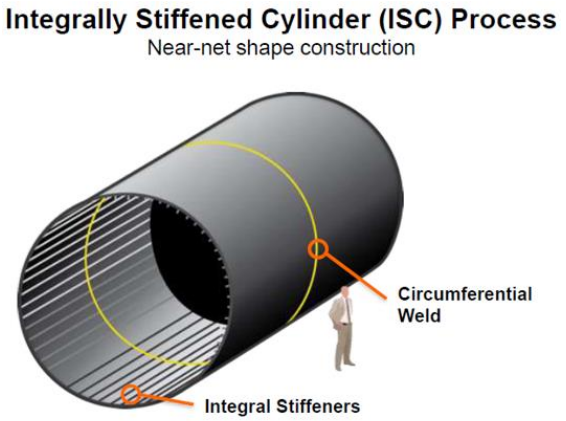

Figure 1. ISC full-scale model, showing integral stiffeners, and attachment welds between ISCs[4].

In this work, the development of a robust FEM for spin and flow forming of Al 6061 in a WF Maschinenbau VUD-600 is being pursued. The system is capable of both spin forming (into free space) and flow forming (against a mandrel) in sequential operations. A flat preform is subjected to spin forming deformation (diameter reduction/thickness

constant) prior to contact with the mandrel. Subsequently, the partially-formed part is subjected to flow forming deformation (thickness reduction/diameter constant) along the mandrel. Any simulation of this fabrication process must account for this transition in the type of deformation.

DEFORM® is a continuum-level, deformation modeling suite capable of simulating metal forming processes. The commercial forging software can be used to predict stress and strain distributions or gradients based on processing parameters and material characteristics[8]. This application involves the development of a model that predicts material response, flow defects, and forming loads as a function of spin/flow forming conditions for a specific alloy/temper combination. Certified tensile yield strength and flow stress curves for the Al alloy of interest will be imported for elastic-plastic modeling. The solver is robust, with multiple convergence criteria, particularly for the implicit solvers. The FEM will be formulated to assess the stress or strain distribution, and damage accumulation that occurs during flow forming of a sub-scale component.

The FEM will be calibrated, verified, and validated with experimental evidence to develop the most descriptive model possible. A suitable balance of computational speed and accuracy must be achieved with any FEM. The chosen mesh, solver, material model, and dimensions will yield different results, with varying degrees of accuracy and computational speed within the DEFORM® framework. Model calibration and verification will be performed after selected individual flow forming passes. Additional verification and validation will be performed at the end of the complete forming protocol.

2. Methodology

2.1. Experimental Flow Forming

Parametric studies of flow forming were conducted using the WF VUD-600 vertical flow-forming machine located at NASA Langley Research Center. The configuration of the system, with relevant components labeled, is shown in Figure 2.

The standard forming protocol, developed by

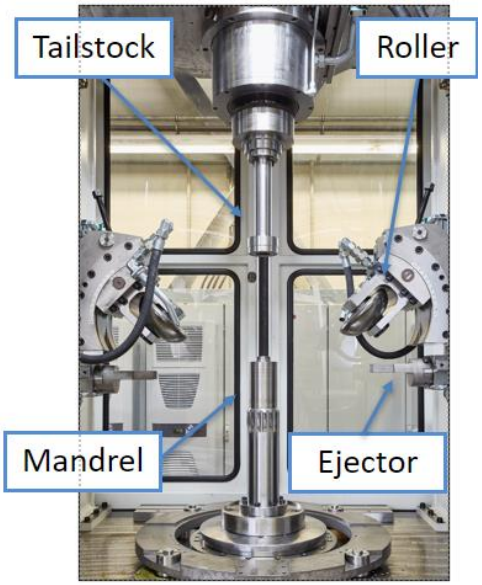

Figure 2. VUD-600 flow forming machine with labeled components.

WF to demonstrate the capabilities of the VUD-600, subjects a disk-shaped metallic preform to five spin forming passes, which reshapes the preform into a cylinder, while keeping the part thickness constant. The partially-formed part then undergoes two forward flow forming passes, reducing the wall thickness and lengthening the overall part. The second forward flow forming pass forces material over a series of grooves on the mandrel, creating integral stiffeners on the flow formed part. A reverse flow forming step then further thins the wall thickness of the cylinder. The final step reduces the

diameter near the top to form a discrete necked-in region. The whole sequence of steps from the flat plate preform to fully-formed part is illustrated in Figure 3.

Figure 3. Top and side views of the incremental forming steps using the VUD 600 standard protocol.

Three 10-mm-thick Al 6061 disks were formed, stopping the forming process after the first spin pass, last spin pass, and after flow forming for experimental support and validation. In-situ force measurements on the rollers were recorded for each experimental disk, and each preform was inspected after forming for surface defects and blemishes. The experimental geometries were also determined through structured blue-light scanning, which has a resolution of 3 µm. The full outer geometry of the three experimental parts was captured as point cloud data, which can be used to compute cross-sectional geometry, eccentricity of the part, plus variations in the thickness.

2.2. Finite Element Model Development

Plastic deformation FEMs for metal forming have been utilized for decades, but have only recently been applied to flow and spin forming[7]. The discretized element nodes are incrementally solved for displacement and velocity based on material flow curves in plastic deformation FEMs. The tensile flow curves for Al 6061 in the -O temper, shown in Figure 5, were used at strain rates of 0.1–10 s^{-1} for the present work[8].

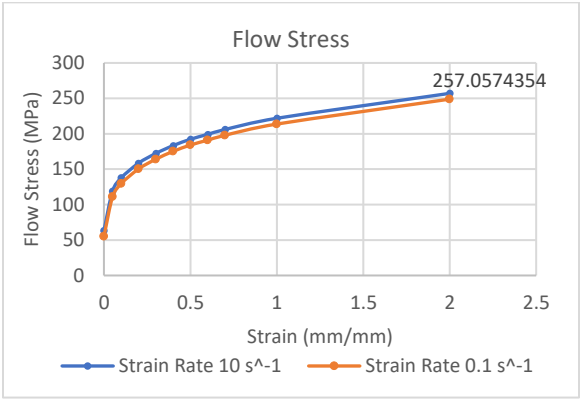

Figure 5. Al 6061-O flow stress curves used in DEFORM® plastic deformation models.

The FEM was developed using the parameters in the standard forming protocol of the VUD-600, outlined in Section 1. An overview of the current setup is shown in Figure 5, with the location of the 220-mm-diameter by 10-mm-thick preform depicted as a blue disk. The material and deformation equations are only simulated on the blue preform. All other geometries (rollers, tailstock, mandrel) are meshed to provide contact boundary points for the preform, but are not iteratively updated. The path of the roller centroid for spin forming is shown in

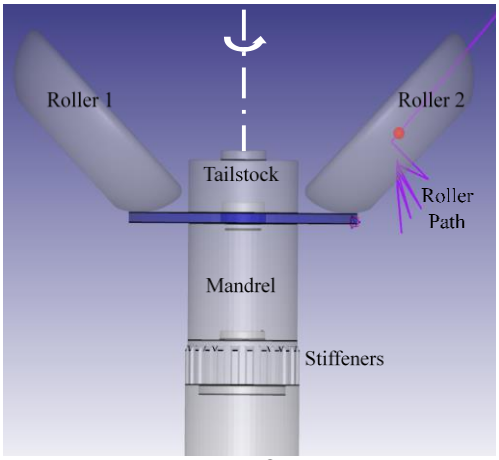

Figure 4. DEFORM® VUD-600 model.

purple. Through the length of the simulation, the mandrel rotation rate varies between 300–400 rpm, with a roller translation speed of 800–3000 mm/min.

The FEM assumed isothermal conditions and was developed using a three-dimensional (3D) implicit Lagrangian solver, with 150,000 tetrahedral elements. The model was run using elasto-plastic material properties to account for spring-back and residual stresses. The average element edge length was 2.4 mm. The time step was chosen to be 0.5 ms, so the model iterated approximately 300 times per mandrel revolution.

3. Results

3.1. Model Verification

Each time step took 43 computational seconds to run with the current configuration, and the full five-pass spin forming simulation ran for approximately 3 weeks. A grid convergence study was performed to determine the mesh size needed for accuracy. As shown in Figure 6, doubling the number of elements from 107246 elements to 240228 elements did not change the stress field shape, but consistently yielded maximum stress values 7 MPa to 10 MPa higher, a 0.5% difference in maximum stress.

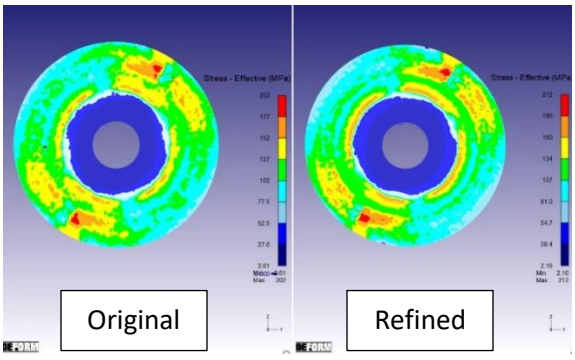

Figure 6. Effective stress fields at the original and refined mesh sizes, showing minimal differences to the global stress maps.

The difference in plastic deformation solvers was considered, in addition to convergence investigations. The different solvers included implicit and explicit time schema, plus plastic or elasto-plastic material properties. The solver matrices consisted of Lagrangian, Arbitrary Lagrangian - Eulerian (ALE) and Eulerian solver matrix methods. The 1st spin pass simulations for ALE and Lagrangian solvers are shown in Figure 4, plus a dual-domain and two-dimensional simulation. Although the simulations were performed for the same time step and mesh, the variation of solvers and material types yielded different geometries. Calibration of the FEM to the experimental work ensured selection of the most accurate model.

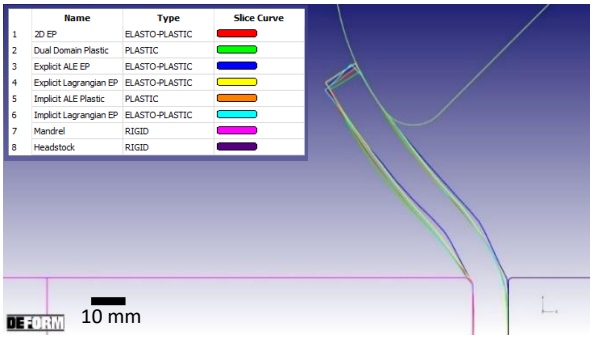

Figure 7. DEFORM® solvers demonstrating differences in predicted geometry for model calibration.

3.2. Model Validation

The model validation and experimental comparison used geometric cross-sections, roller load forces, and qualitative failure analysis. A typical measured cross section and the cross-section predicted by the

simulation of the corresponding time step are compared in Figure 8.

The part geometries in Figure 8 indicate that the experimental and computational cross-sections generally have good agreement. The computational cross-section predicted more radial thinning and elongation than occurs experimentally. However, many of the experimental features were captured within the computational model. These included the peak near the clamped region, the general thinning through the radial cross-section, and the beveled flange at the free edge of the formed part.

In conjunction with the geometric cross-sections, the forces exerted by the rollers computationally and experimentally are plotted in Figure 9. While the magnitudes of the experimental data were generally half that

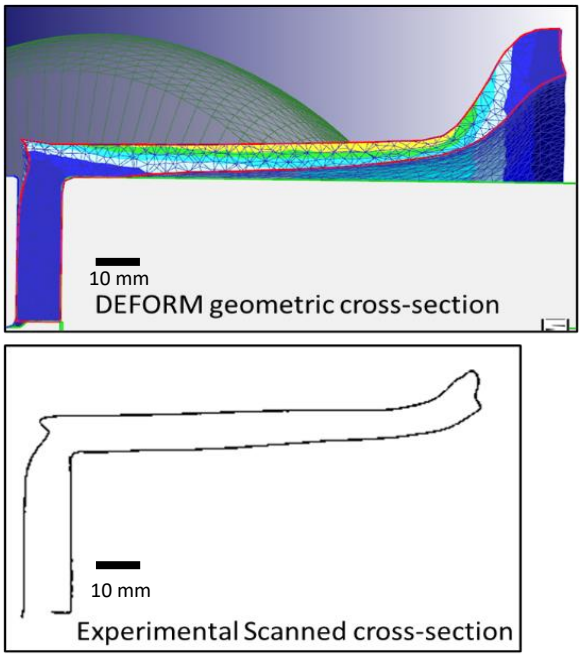

Figure 8. Geometric cross-section comparison between DEFORM® model and 3D scanned experimental part

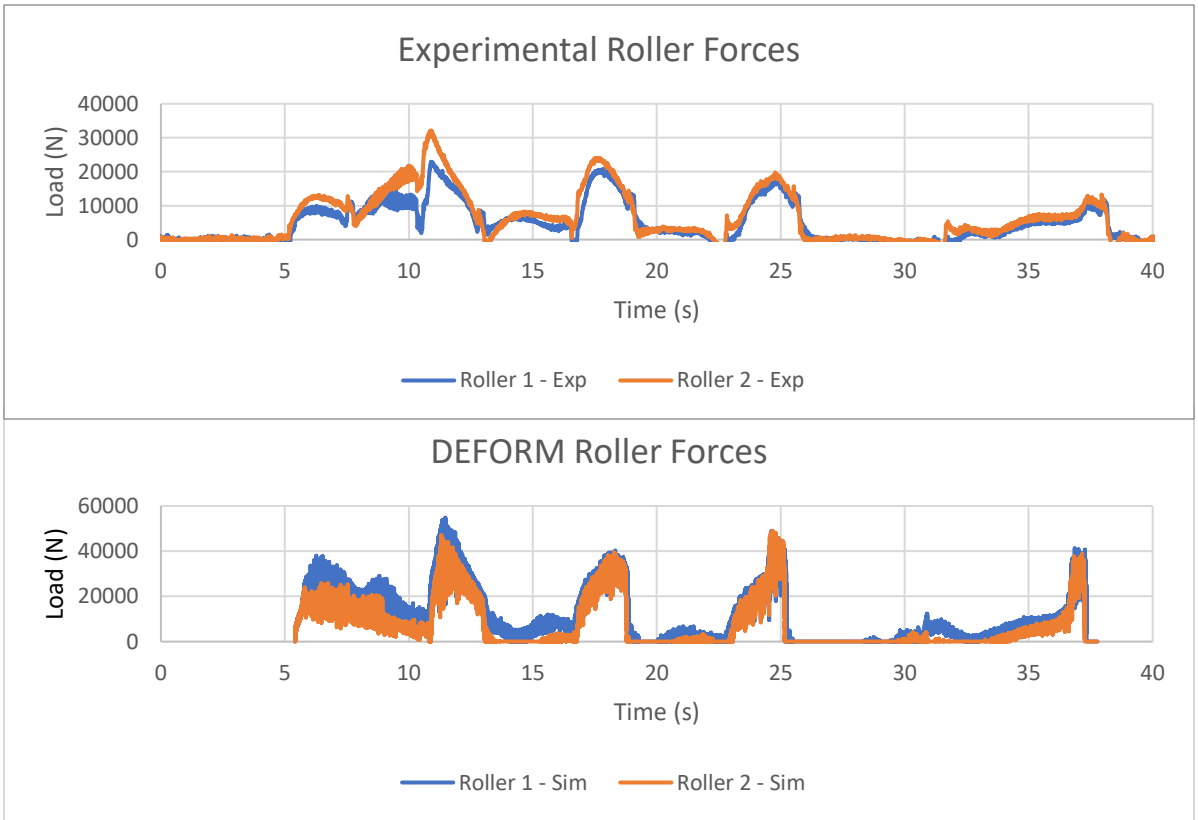

Figure 9. Roller forces determined experimentally and computationally show variance in magnitude, but agreement in local maxima and shape.

of the computational model, the relative shape trends and extrema correlate well.

Finally, identifying the location of failure initiation was considered. Failure criteria were the most qualitative of the validation techniques used. A post-forming review of the FEM was conducted when an experimental part failed prematurely (Figure 10). The most likely failure location predicted by the Cockcroft-Latham damage criteria tended to align with the actual location of failure.

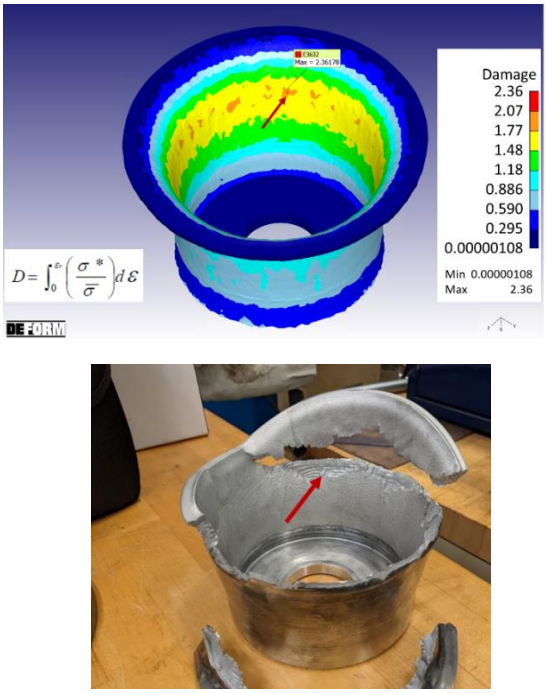

Figure 10. Computational Cockcroft-Latham damage prediction compared to experimental failure.

4. Discussion

While the model and experiment are generally in good agreement, the results could be refined. The computational model exhibits limitations; the most crucial being the time dependency of the model. At 3 weeks of computational time, the interval required to run the model is ≥ 500 hours. DEFORM® only allows for parallelization up to 16 cores, dramatically limiting the speed a model can be solved. Additional limiting factors include the simplifying assumptions, such as assuming that the system is isothermal, with no heat transfer occurring, and that the model accurately captures all the features needed. The throttled computational time also limits the element size and mesh refinement that can occur, which casts doubt on the usefulness of the model for manufacturing operations.

In addition, the Al 6061 material properties extracted from the literature are assumed to be accurate. Further property evaluation may be needed to quantify the material flow fields for the specific material utilized for VUD-600 flow forming.

The comparison and accuracy of roller forces and geometric cross-sections are not exact. The discrepancy may be due to differences in material flow paths or compounding of discretization errors and simplifying assumptions.

A key result of this computational work was that the improved understanding of the process provided better direction to the experimental work. The Cockcroft-Latham damage criteria successfully predicted tensile crack initiation sites based on material properties, and history of plastic stain and stress history at a particular location.

The loading and strain history of the spun-formed part was not purely tensile, so literature numerical values indicating failure do not translate. However, the general trend that higher values are more likely to fail holds true, which can provide key insights into alternate designs for flow forming.

5. Conclusions

Based on this work, three key conclusions on the development of a plastic deformation computational model can be drawn:

1. The FEM represented an appropriate balance between accuracy and speed.
2. The FEM showed reasonable agreement between predicted and measured part geometry and roller loads.
3. The FEM demonstrated the ability to qualitatively locate regions of probable failure.

6. Future Work

There are several key avenues that will be pursued for the development and advancement of the work presented. Further validation, including destructive characterization, will be performed to quantify residual stresses and plastic strain within the cross-sections. Such validation will aid understanding the computational model more thoroughly, in terms of both predictions and limitations.

A validated model will permit further investigation of the stiffener region. Specifically, the formation of the stiffeners will be evaluated. Potential geometries for thinner and taller stiffeners will be pursued.

References

1. Tayon, W., Domack, M., Wagner, J.: Characterization of 10-ft. Diameter Aluminum Alloy 2219 Integrally Stiffened Cylinders. NASA/TM-2019-220260 (2019)
2. Zell, D., Domack, M., Tayon, W., Stachulla, M., Wagner, J.: Low Cost Manufacturing Methods. In: Technologies for Future Space Transportation Systems. Washington D.C. (2019)
3. Tayon, W., Newman, S., Domack, M.: Characterization of Aluminum 6061 Integrally Stiffened Cylinder. Presented at the Strategic Interchange Meeting, NASA Langley Research Center April 11 (2017)
4. Stoner, M.C., Hehir, A.R., Ivanco, M.L., Domack, M.S.: Cost-Benefit Analysis for the Advanced Near Net Shape Technology (ANNST) Method for Fabricating Stiffened Cylinders. (2016)
5. Mohebbi, M.S., Akbarzadeh, A.: Experimental study and FEM analysis of redundant strains in flow forming of tubes. J. Mater. Process. Technol. 210, 389–395 (2010). https://doi.org/10.1016/j.jmatprotec.2009.09.028
6. Jiang, S., Zheng, Y., Ren, Z., Li, C.: Multi-pass spinning of thin-walled tubular part with longitudinal inner ribs. Trans. Nonferrous Met. Soc. China. 19, 215–221 (2009). https://doi.org/10.1016/S1003-6326(08)60255-1
7. Kobayashi, S., Oh, S.-I., Altan, T.: Metal forming and the finite-element method. Oxford University Press, New York (1989)
8. DEFORM V12.1.1 Manual: Scientific Forming Technologies Corporation, Columbus, OH, Officially released; June 18, 2021.*

* The use of trademarks or names of manufacturers in this report is for accurate reporting and does not constitute an official endorsement, either expressed or implied, of such products or manufacturers by the National Aeronautics and Space Administration.